



Original Article

A computed tomography (CT)-based morphometric study of various skull base parameters and their anatomical relationships relevant to endoscopic endonasal skull base surgery

Ganesh V. L¹, Sundarakrishnan Dharanipathy¹, Pavana V¹, Amandeep Kumar¹, Leve Joseph Devarajan Sebastian², Ajay Garg²

Departments of ¹Neurosurgery and ²Neuroradiology, All India Institute of Medical Sciences, New Delhi, Delhi, India.

E-mail: Ganesh V. L - ganeshmedicorockz@gmail.com; Sundarakrishnan Dharanipathy - radnus23@gmail.com; Pavana V - vppavana@gmail.com; *Amandeep Kumar - aman_jagdevan@yahoo.co.in; Leve Joseph Devarajan Sebastian - leve_s@yahoo.com; Ajay Garg - drajaygarg@gmail.com



***Corresponding author:**

Amandeep Kumar,
Department of Neurosurgery,
All India Institute of Medical
Sciences, New Delhi, Delhi,
India.

aman_jagdevan@yahoo.co.in

Received: 22 December 2023

Accepted: 02 February 2024

Published: 01 March 2024

DOI

10.25259/SNI_1010_2023

Quick Response Code:



ABSTRACT

Background: Endoscopic skull base surgery requires a thorough understanding of skull base anatomy. Orientation to regional anatomy to avoid complications like internal carotid artery injury can be assisted by knowledge of certain bony landmarks. These landmarks are themselves highly variable structures. This study focuses on the radiological morphometric characterization of these landmarks, which can be of great assistance to surgeons for better planning of endoscopic skull base approaches.

Methods: Computed tomography scans of patients without skull base pathologies were analyzed retrospectively for the following parameters – Vidian canal (VC) length, VC and foramen rotundum (FR) distance from midline, the angle between the axis of VC and petrous internal carotid artery (pICA) and between VC and palatovaginal canal, the horizontal, vertical and direct distances between VC and FR and the patterns of sphenoid sinus (SS) pneumatization.

Results: The VC-pICA angle was more obtuse and VC and FR were placed farther off the midline on the left as compared to the right side. Similarly, the distances between VC and FR were more on the left side. The VC length and distance of VC and FR from the midline were longer in males than in females. The VC-pICA angle was more obtuse in females. The post-sellar variant was the predominant pneumatization pattern seen (57.9%), and the incidence of lateral recess pneumatization was 15%.

Conclusion: The results of our study can be utilized for a better understanding of the anatomy of the skull base. In skull base pathologies with distorted anatomical landmarks, a basic understanding of their interrelations can be used to have a better anatomical orientation. All these measures can help in avoiding complications and make extended endoscopic approaches safe.

Keywords: Endoscopic skull base surgery, Extended endoscopic approaches, Foramen rotundum, Petrous internal carotid artery, Vidian canal

INTRODUCTION

Knowledge about anatomy paves the way for surgery. The radiological correlation of anatomy and its intraoperative application can be compared to driving a road with good-quality navigation. As

This is an open-access article distributed under the terms of the Creative Commons Attribution-Non Commercial-Share Alike 4.0 License, which allows others to remix, transform, and build upon the work non-commercially, as long as the author is credited and the new creations are licensed under the identical terms.

©2024 Published by Scientific Scholar on behalf of Surgical Neurology International

the road carries certain signboards to avoid accidents, certain bony structures can be considered signboards for safely accessing the skull base. The complexity of skull base anatomy and intricate interrelations between important neurovascular structures make skull base endoscopic surgery a challenging field. As the internal carotid artery (ICA) is unavoidably encountered during extended endoscopic approaches (EEAs), its injury is the most feared complication. Identification of petrous internal carotid artery (pICA) and cavernous ICA is thus a crucial step in EEAs. One important anatomical landmark that can assist surgeons in identifying foramen lacerum (FL) and petrous ICA is the Vidian canal (VC), which can be localized during the early stages of exposure in EEAs.^[15] The VC is a narrow bony pathway for the passage of the Vidian nerve, which in turn is formed by the union of greater petrosal and deep petrosal nerves.^[10,21] VC plays a paramount role in identifying the anterior genu of petrous ICA, which is helpful in intraoperative avoidance of vascular complications.^[4,11,15] VC is highly variable in its position and relation to other anatomical structures, especially the petrous ICA and foramen rotundum (FR).^[8,15] In addition, the sphenoid sinus (SS), which is the natural corridor to access the sellar and parasellar regions, is the most variable cavity in the human body and variations in pneumatization patterns of SS have a great bearing on the level of difficulty encountered during the exposure of skull base in EEAs. Thus, to have a better understanding of the anatomical orientation for the avoidance of intraoperative complications, it is critical to understand the morphometric features of VC and its relations to surrounding structures and the variations in pneumatization patterns of SS preoperatively. The present study aims to analyze various computed tomography (CT) based radiological morphometric features of the VC and its relationship with petrous ICA and FR in addition to the variations in SS pneumatization patterns in the normal population. The study will help in the identification and recognition of variations in pertinent skull base bony landmarks relevant to endoscopic skull base surgery.

MATERIALS AND METHODS

This was a retrospective cross-sectional study conducted at a tertiary care center. Patients who had undergone CT scans for indications other than skull base pathologies, skull base fractures, and sinonasal pathologies and those who had not undergone previous skull base surgical intervention were identified. From this cohort, patients with 1 mm slice thickness CT scans were then included in the study. Only adult patients with an age of more than 18 years were included in the study. The images were retrieved from our picture archiving and communication system (PACS). All CT scans were performed using the Siemens Somatom Definition Edge multidetector CT (128 slice) scanner. The CT imaging protocol was as

follows: gantry speed - 0.28 s/rotation, collimation 128 × 0.6 mm, table increment - 5 mm/, parameters - 100 kV, and effective mAs 430–490. Sections were reconstructed with 1 mm section thickness with zero interval in bone window settings for studying the skull base bony anatomy.

CT scans of patients meeting eligibility criteria were assessed independently by a neurosurgeon and a neuroradiologist. In cases with discordant findings, the images were re-evaluated to reach a consensus. For each included patient, the following measurements from both the right and left sides were measured using GEPACS software in axial, sagittal, and coronal planes [Figures 1-3].

Length of VC

The length of VC was measured in the axial plane. To determine the length of VC, a line was drawn through the center of VC from its anterior to the posterior end [Figure 1a].

VC-pICA angle

This was defined as the angle subtended between the axis of VC and that of the petrous carotid canal. It was measured in axial images. A line was drawn along the axis of VC. Another line was drawn along the axis of the petrous carotid canal at the level of VC. The angle subtended at the point where these two lines meet was measured and was termed the VC-petrous ICA angle [Figure 1b].

VC-palatovaginal canal (PVC)

This was defined as the angle subtended between the axis of the VC and that of the PVC. It was measured in axial images. A line was drawn along the axis of VC. Another line was drawn along the axis of the PVC at the level of VC. The angle subtended at the point where these two lines meet was measured and was termed the VC-PVC angle [Figure 1c].

Distance of VC and FR from the midline

An imaginary vertical line was drawn along the midline. Then, a line parallel to the midline and passing through the center of VC was drawn. The distance between these two lines gave the distance of VC from the midline. Similarly, the distance of FR from the midline was determined [Figure 2a].

VC-FR distance

The distance between VC and FR was measured on coronal images. The shortest vertical distance between VC and FR was determined by drawing two horizontal lines passing through the centers of VC and FR. The distance between these two lines gave us the shortest vertical distance between VC and FR. The direct distance between VC and FR was also

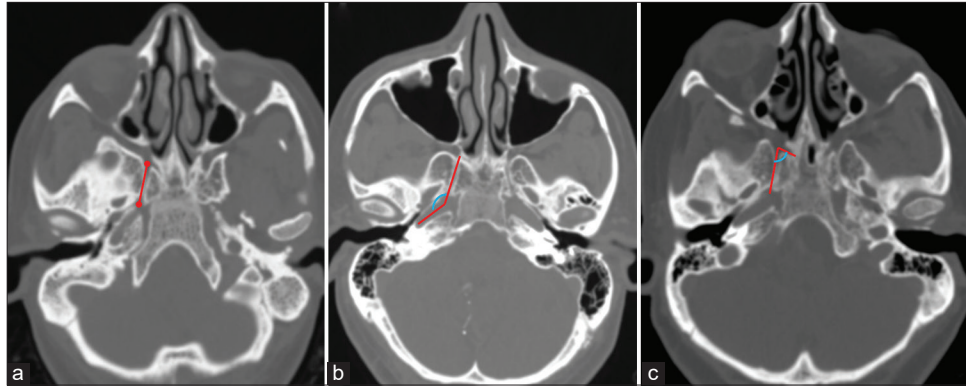


Figure 1: Axial computed tomography images showing the method used to measure (a) Vidian canal (VC) length (represented by red line), (b) VC-petrous internal carotid artery angle (represented by blue curved line between two red lines), and (c) VC-palatovaginal canal angle (represented by blue curved line between two red lines).

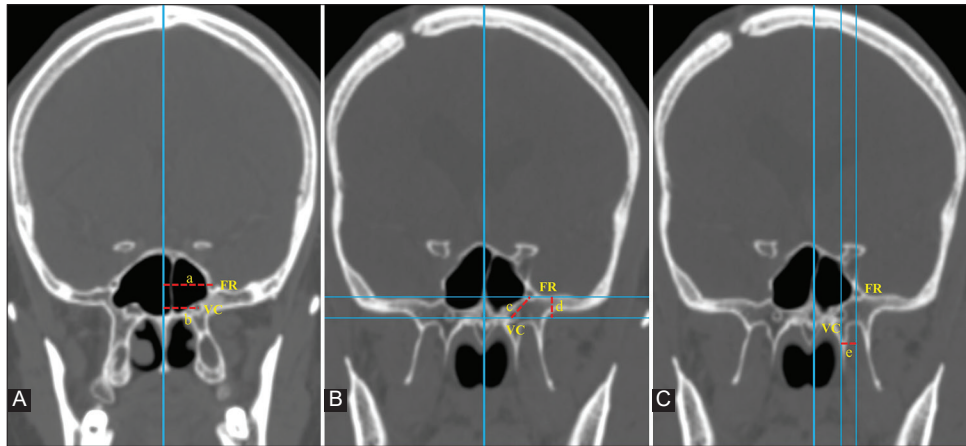


Figure 2: In coronal computed tomography images, a vertical imaginary line is drawn in the midline along the vomer bone. (A) Distance of foramen rotundum (FR) and Vidian canal (VC) from the midline is measured (represented by 'a' and 'b' respectively). (B) Two horizontal lines are drawn, crossing the midpoint of VC and FR. The vertical distance between these two lines gives the vertical distance between FR and VC (represented by 'd'). The direct distance between VC and FR (represented by 'c') is then measured. (C) The horizontal distance between VC and FR is measured as the distance between two vertical lines drawn across the centers of the two foramina (represented by 'e').

measured in this coronal image [Figure 2b]. To determine the horizontal distance between VC and FR, a vertical line was drawn along the midline. Then, two vertical lines were drawn parallel to the first line but passed through the centers of FR and VC. The distance between these two lines represented the shortest horizontal distance between VC and FR [Figure 2c].

SS

SS pneumatization is highly variable. These variations are very diverse and frequent. We analyzed SS pneumatization for the following variations [Figures 3a-c]:

In the sagittal plane

In mid sagittal section, two tangents are drawn from the anterior and posterior walls of the pituitary fossa.

- i. Conchal type—when the sinus is non-pneumatized
- ii. Presellar type—when the pneumatization extends to the anterior line
- iii. Sellar type—when the pneumatization extends to a point between two lines
- iv. Postsellar type—when the pneumatization extends posteriorly to the second line.

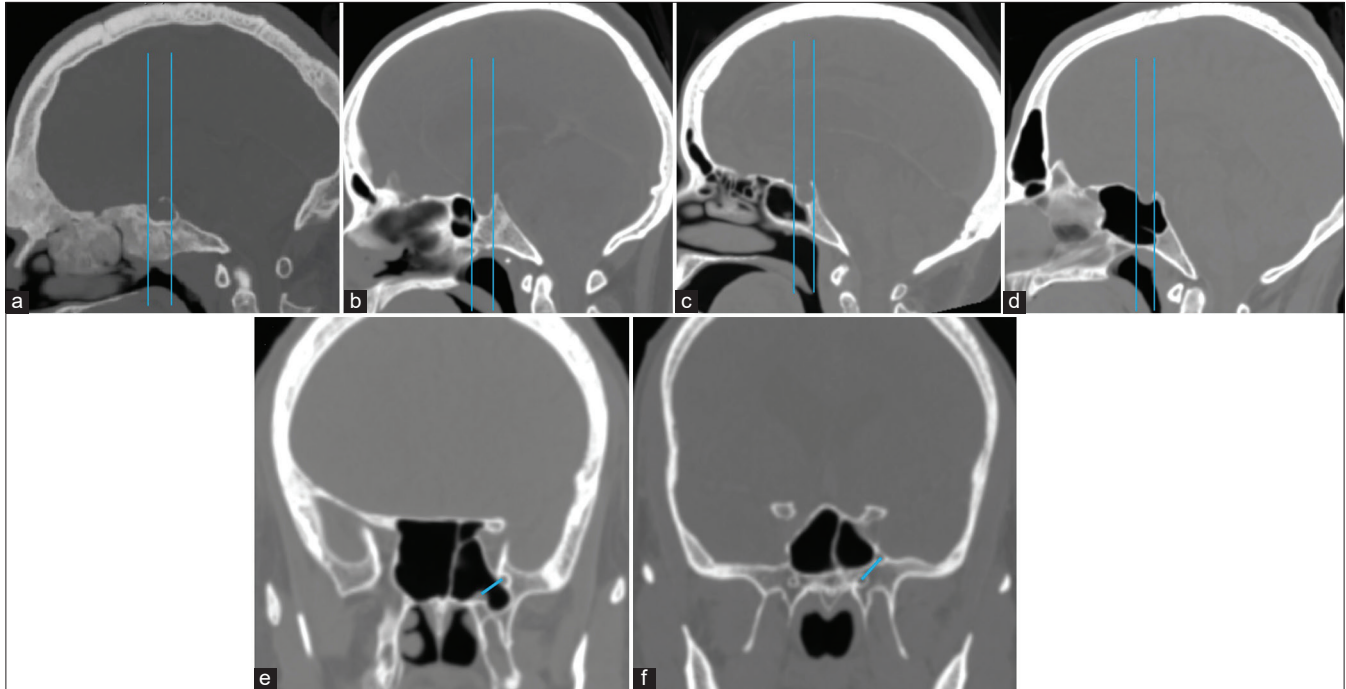


Figure 3: (a-c) In sagittal computed tomography images, the two vertical lines drawn along the anterior and posterior walls of the pituitary fossa determine the type of SS pneumatization in a sagittal plane, which is classified as (a) Conchal, (b) Presellar, (c) Sellar, and (d) Postsellar types. (e and f) An oblique line connecting the centers of the Vidian canal and foramen rotundum determines the presence (d) or absence (e) of lateral recess pneumatization.

In the coronal plane

Lateral recess pneumatization was classified into three types based on an imaginary oblique line connecting the medial edge of the anterior opening of VC and FR [Figures 3d and e].

- i. Nonpneumatized–Sphenoid body pneumatization without lateral extension
- ii. Pneumatized lateral recess–Pneumatization extending beyond the oblique line described above
- iii. Pneumatization extends into the lesser wing of the sphenoid/anterior clinoid process.

Statistical analysis

The data were analyzed using the STATA 16.0 (Stata Corp, College Station, TX) software. Categorical variables are presented as *n* (%), and continuous variables are presented as mean (standard deviation [SD]) or median (interquartile range) as applicable. Categorical variables were compared using the Fisher exact test or Chi-square test, wherever applicable, and continuous variables were compared using an independent sample Student's *t*-test. Statistical significance was set at $P < 0.05$.

RESULTS

A total of 473 individuals who had undergone CT scans between January 2020 and December 2022 were included

in the study. There were 263 males (55%) and 210 females (45%) in the study. The mean age was 40.91 ± 13.6 years in males and 42 ± 12.96 years in females ($P = 0.377$).

Baseline parameters

Baseline parameters were calculated after combining both sides ($n = 946$). The mean and median lengths of VC were 14.71 mm (SD–1.77) and 14.7 mm, respectively. The mean and median angles between VC and PVC were 60.99° (SD–10.25) and 61.2° , respectively. The mean and median angles between VC and petrous ICA were 138.07° (SD – 6.89) and 138.4° , respectively. The mean and median distances of VC from the midline were 12.10 mm (SD – 1.51) and 12 mm, respectively. The mean and median distances of FR from the midline were 18.27 mm (SD – 2.30) and 18.4 mm, respectively. The mean and median horizontal distances between FR and VC were 6.21 mm (SD – 1.76) and 6.2 mm, respectively. The mean and median vertical distances between VC and FR were 4.53 mm (SD – 1.77) and 4.4 mm, respectively. The mean and median direct distances between VC and FR were 7.89 mm (SD – 1.98) and 7.6 mm, respectively [Table 1].

Skull base parameter–right versus left

The average lengths of VC on the right and left were 14.77 ± 1.82 and 14.65 ± 1.72 , respectively ($P = 0.290$). The angle

Table 1: Baseline skull base parameters.

	Mean	Standard deviation	Median	Minimum	Maximum	Quartile-1	Quartile-3
VC Length (in mm)	14.71	1.77	14.7	8.5	19.8	13.4	16
VC-PVC angle (°)	60.99	10.25	61.2	29.2	95.1	53.7	68.3
VC-pICA angle (°)	138.07	6.89	138.4	115.4	159	133.8	142.7
Midline-VC distance (in mm)	12.10	1.51	12	7.5	19.1	11.1	13
Midline-FR distance (in mm)	18.27	2.30	18.4	6.8	29.4	16.8	19.8
VC-FR horizontal distance (in mm)	6.21	1.76	6.2	1.8	15.4	5	7.4
VC-FR vertical distance (in mm)	4.53	1.77	4.4	1	13.3	3.3	5.6
VC-FR direct distance (in mm)	7.89	1.98	7.6	4	18	6.5	9

VC: Vidian canal, FR: Foramen rotundum, PVC: Palatovaginal canal, pICA: Petrous internal carotid artery

Table 2: Side-wise comparative analysis of various skull base parameters.

	Right (Mean±SD)	Left (Mean±SD)	P-value	Odds ratio with 95% CI
VC Length (in mm)	14.77±1.82	14.65±1.72	0.290	-
VC-PVC angle (°)	61.64±10.67	60.35±9.78	0.052	-
VC-pICA angle (°)	137.39±6.95	138.75±6.78	0.002	0.97 (0.95–0.99)
Midline-VC distance (in mm)	11.92±1.47	12.3±1.54	0.0001	0.85 (0.77–0.92)
Midline-FR distance (in mm)	17.88±2.29	18.66±2.24	0.000	0.86 (0.81–0.91)
VC-FR horizontal distance (in mm)	6.04±1.65	6.39±1.85	0.002	0.89 (0.83–0.96)
VC-FR vertical distance (in mm)	4.35±1.74	4.72±1.79	0.002	0.89 (0.83–0.96)
VC-FR direct distance (in mm)	7.65±1.85	8.12±2.07	0.0002	0.88 (0.83–0.94)

VC: Vidian canal, FR: Foramen rotundum, SD: Standard deviation, CI: Confidence interval, PVC: Palatovaginal canal, pICA: Petrous internal carotid artery

between the VC and PVC was 61.64 ± 10.67 mm on the right and 60.35 ± 9.78 mm on the left side ($P = 0.052$). The angle between pICA and VC was $137.39^\circ \pm 6.95^\circ$ on the right and $138.75^\circ \pm 6.78^\circ$ on the left side ($P = 0.002$). The distance of the VC from the midline measured on the right and left were 11.92 ± 1.47 and 12.3 ± 1.54 , respectively ($P = 0.0001$). The distance of FR from the midline was 17.88 ± 2.29 on the right and 18.66 ± 2.24 on the left side ($P = 0.000$). The horizontal distances between VC and FR on the right and left were 6.04 ± 1.65 and 6.39 ± 1.85 , respectively ($P = 0.002$) with odds of 0.89 (0.83–0.96; 95% confidence interval [CI]). The vertical distance between VC and FR on the right and left was 4.35 ± 1.74 and 4.72 ± 1.79 ($P = 0.002$), with an odds ratio of 0.89 (0.83–0.96; 95% confidence interval [CI]). The direct distance between VC and FR on the right and left was 7.65 ± 1.85 and 8.12 ± 2.07 , respectively ($P = 0.0002$), with an odds ratio of 0.88 (0.83–0.94; 95% CI) [Table 2].

Skull base parameters—males versus females

A subgroup analysis of morphometric parameters was done to analyze sex-specific variations. The mean length of VC was 15 ± 1.8 and 14.4 ± 1.7 , respectively, in males and females ($P = 0.001$), and the odds ratio with 95% CI was 0.82 (0.77–0.9). The angle between VC and PVC in males and females was 60.8 ± 10 and 61.2 ± 10.5 , respectively ($P = 0.5$). The angle between VC and Petrous ICA in males and females

was 137.4 ± 7.2 and 139 ± 6.4 , respectively ($P = 0.0003$). The distance of VC from the midline in males and females was 12.5 ± 1.5 and 11.6 ± 1.4 , respectively ($P < 0.001$), and the odds ratio with 95% CI for the same was 0.66 (0.6–0.73). The distance of FR from the midline in males and females was 18.6 ± 2.3 and 17.8 ± 2.2 ($P < 0.001$), with an odds ratio of 0.84 (0.8–0.9). The horizontal distance between VC and FR in males and females was 6.2 ± 1.8 and 6.2 ± 1.7 , respectively ($P = 0.9$). The vertical distance between VC and FR in males and females was 4.6 ± 1.9 and 4.4 ± 1.6 , respectively ($P = 0.06$). The direct distance between VC and FR in males and females was 8 ± 2.1 and 7.8 ± 1.8 , respectively ($P = 0.18$) [Table 3 and Figure 4].

SS pneumatization

In our study, the post-sellar variant was the predominant pneumatization pattern seen in 57.9% ($n = 274$), followed by the seller variant in 24.3% ($n = 115$). The presellar and conchal were found in 17.6% ($n = 83$) and 0.2% ($n = 1$), respectively.

The lateral recess pneumatization was seen in 14.6% ($n = 69$) of the patients on the right side and 15.4% ($n = 73$) on the left side. The pneumatization beyond the lateral recess into the greater wing of the sphenoid or clinoid process was observed in 2.5% ($n = 12$) on the right and 4.5% ($n = 21$) on the left side [Tables 4 and 5 and Figure 5].

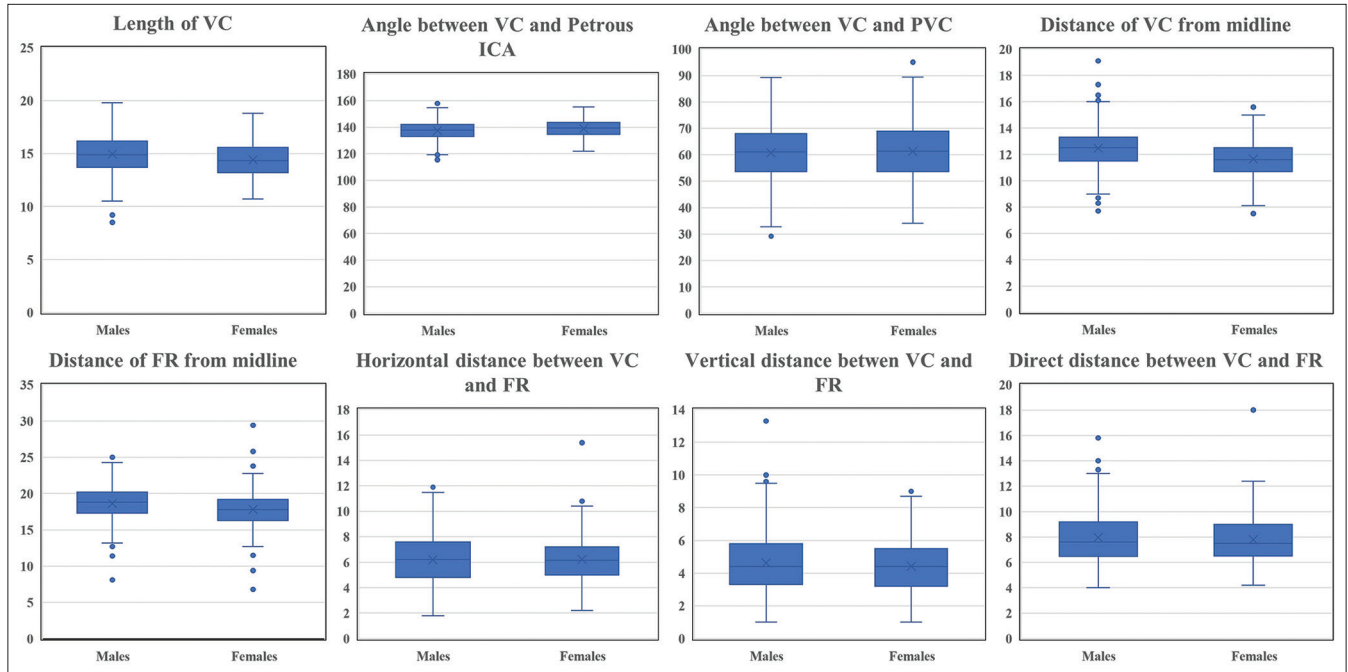


Figure 4: Box plot graphs showing gender-wise comparative analysis of various skull base parameters. VC: Vidian canal; ICA: Internal carotid artery; PVC: Palatovaginal canal; FR: Foramen rotundum.

Table 3: Gender-wise comparative analysis of various skull base parameters.

	Male (mean±SD)	Female (mean±SD)	P-value	Odds ratio with 95% CI
VC length (in mm)	15±1.8	14.4±1.7	<0.001	0.82 (0.77–0.9)
VC-PVC angle (°)	60.8±10	61.2±10.5	0.5	-
VC-pICA angle (°)	137.4±7.2	139±6.4	0.0003	1.03 (1.02–1.06)
Midline-VC distance (in mm)	12.5±1.5	11.6±1.4	<0.001	0.66 (0.6–0.73)
Midline-FR distance (in mm)	18.6±2.3	17.8±2.2	<0.001	0.84 (0.8–0.9)
VC-FR horizontal distance (in mm)	6.2±1.8	6.2±1.7	0.9	-
VC-FR vertical distance (in mm)	4.6±1.9	4.4±1.6	0.06	-
VC-FR direct distance (in mm)	8±2.1	7.8±1.8	0.18	-

VC: Vidian canal, FR: Foramen rotundum, SD: Standard deviation, CI: Confidence interval, PVC: Palatovaginal canal, pICA: Petrous internal carotid artery

Table 4: Sphenoid sinus pneumatization patterns on sagittal images.

Sphenoid sinus	Total (n/%)	Male (n/%)	Female (n/%)
Conchal	1 (0.2)	1 (0.4)	0
Presellar	83 (17.6)	44 (16.7)	39 (18.6)
Sellar	115 (24.3)	53 (20.1)	62 (29.5)
Postsellar	274 (57.9)	165 (62.7)	109 (51.9)
Total	473	263	210

DISCUSSION

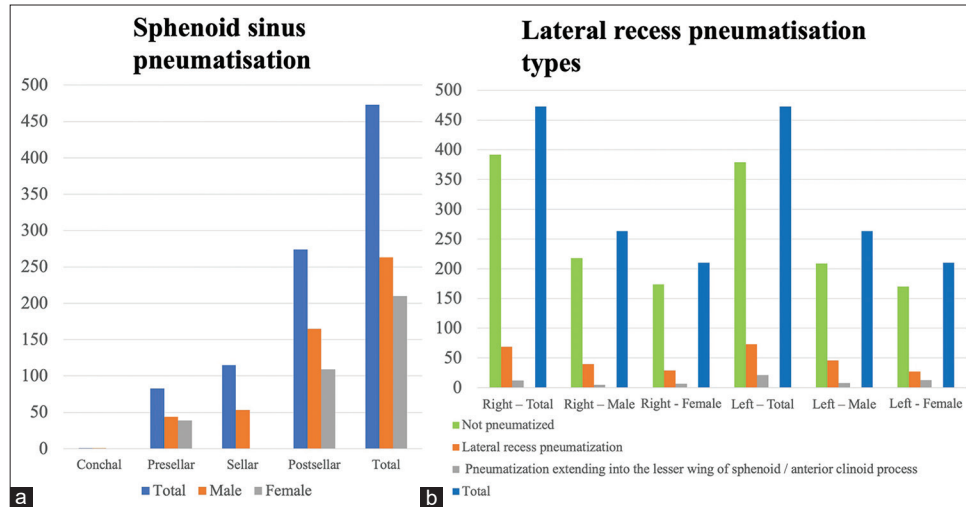
The human skull base can be considered a pinnacle of craftsmanship with minute detailing to satisfy the purpose of various structures. There are various foramina through which neurovascular structures enter or exit the brain,

and foramina can be widely used as a landmark for skull base surgery. The anterior opening of VC and FR are two important foramina that are crucial for anatomical orientation in the region. The VC is a reliable landmark to identify the pICA as well as the cavernous sinus and the Meckel’s cave.^[4,11,12,16,22] The VC opens anteriorly into the pterygopalatine fossa (PPF), and following it posteriorly, one leads to FL and thus the pICA. The PVC is a safe and reliable landmark for the identification of VC during endoscopic endonasal trans-ptyergoid approaches. A crucial step in trans ptyergoid approaches is the identification of VC.^[10] This may be difficult in cases where the tumor infiltrates the VC. Furthermore, tumors like nasopharyngeal carcinomas can spread to PPF and can then further spread through VC.^[13] In such a situation, PVC may prove to be a valuable landmark for the localization of VC.^[13,18] In the

Table 5: Lateral recess pneumatization.

Lateral recess	Total (n/%)		Males (n/%)		Females (n/%)	
	Right	Left	Right	Left	Right	Left
Not pneumatized	392 (82.9)	379 (80.1)	218 (82.9)	209 (79.5)	174 (82.9)	170 (80.9)
Lateral recess pneumatization	69 (14.6)	73 (15.4)	40 (15.2)	46 (17.5)	29 (13.8)	27 (12.9)
Pneumatization extending into LWS/ACP	12 (2.5)	21 (4.5)	5 (1.9)	8 (3)	7 (3.3)	13 (6.2)
Total (n)	473	473	263	263	210	210

LWS: lesser wing of sphenoid, ACP: anterior clinoid process

**Figure 5:** (a) Bar charts depicting the distribution of various types of sphenoid sinus pneumatization and (b) lateral recess pneumatization among the study population.

trans pterygoid approach, the PPF is entered after removing the posterior maxillary sinus wall. The sphenoidal process of palatine bone is then removed to expose the palatovaginal artery in PVC, a reliable landmark for VC localization.^[13,18]

The SS has quite variable pneumatization patterns. SS pneumatization has an important bearing on the amount of drilling that is required in EEAs. The presence of a well-pneumatized SS makes it easier to access the Sella and identify important intrasphenoidal landmarks like medial/lateral optico-carotid recess, optic nerve, and cavernous ICA. In the presence of well-pneumatized SS, ON and ICA may be covered with very thin or no bone at all, thereby predisposing these structures to injury during surgery. On the other hand, when there is incomplete or no pneumatization, a lot of drilling is required, which not only increases the operative time but also increases the risk of injury to neurovascular structures (optic nerve, ICA).

VC and its relations

The VC is the conduit for the passage of the Vidian nerve and artery. The paired VCs are present along the line of fusion of

pterygoid processes to the body of the sphenoid. The canal opens anteriorly into the medial part of the PPF and posteriorly at the upper part of the anterolateral edge of the FL.^[2,8]

In our study, the mean length of VC was 14.71 ± 1.77 mm, which is similar to what has been reported in the literature.^[1,12] However, in some studies, VC has been reported to be longer (~ 16.5 mm), which could be due to anthropological differences between different racial populations.^[17] The length of VC on the right and left sides was similar (14.77 ± 1.82 mm and 14.65 ± 1.72 mm, respectively). We also compared the VC length between males and females. The mean length of VC was 15 ± 1.8 mm and 14.4 ± 1.7 mm, respectively, in males and females ($P = 0.001$), and the odds ratio with 95% CI was 0.82 (0.77–0.9). In our study, the mean angle between VC and p-ICA was $137.39^\circ \pm 6.95^\circ$ on the right side and $138.75^\circ \pm 6.78^\circ$ on the left side ($P = 0.002$). VC-pICA angle was more obtuse in females ($139^\circ \pm 6.4^\circ$) as compared to males ($137.4^\circ \pm 7.2^\circ$).

The mean distance of VC from the midline was 12.1 ± 1.51 mm. The mean distance of VC from the midline was

shorter in females (11.6 ± 1.4 mm) as compared with males (12.5 ± 1.5 mm). The more medial location of the anterior opening of the VC was probably responsible for the more obtuse VC-pICA angle seen in females.

All these anatomical parameters have relevance in EEAs. The position of the VC opening in relation to the midline is important to identify the location of the VC opening into PPF intraoperatively. The length of VC assumes importance in determining the extent of bony resection required to access the region of FL/pICA^[7], while the angle between the VC-pICA helps in determining the spatial relationship between the two structures. This information is important for the surgeon to get oriented to the regional anatomy, especially in EEAs directed toward pathologies involving the petrous apex. This VC-pICA angle has not been previously studied in any of the studies in the available literature, and we feel that this is an important parameter for comprehensive orientation to the complex regional anatomy.

FR and its relations

FR is another important landmark in EEAs. The VC-FR distance is a landmark for quadrangular space during EEAs. The quadrangular space is limited medially and inferiorly by ICA, superiorly by the abducens nerve, and laterally by the maxillary division of the trigeminal nerve.^[12] FR-VC distance has also been shown to have strong correlation with the depth of the lateral recess.^[20]

In our study, the mean distance of FR from the midline was 18.27 mm (SD – 2.30), which is similar to the literature reports.^[9,14] The distance of the FR from the midline was 17.88 ± 2.29 on the right side and 18.66 ± 2.24 on the left side ($P = 0.000$). Similar results have been reported by other authors as well.^[9,14] Both Mohebbi *et al.*^[14] and Kasemsiri *et al.*^[9] found the distance of FR from the midline to be more on the left side.

The mean horizontal, vertical, and direct distances between FR and VC were 6.21 mm (SD – 1.76), 4.53 mm (SD – 1.77), and 7.89 mm (SD – 1.98), respectively. The horizontal, vertical, and direct distances between VC and FR were more on the left side as compared with the right side and the difference was statistically significant. Variable findings have been reported in the literature. Kasemsiri *et al.*^[9] and Mohebbi *et al.*^[14] found the VC-FR distances to be similar on the right and left sides, while Papavasileiou *et al.*^[17] reported the VC-FR distances to be more on the left side, similar to the findings in our study.

The FR was more laterally placed in males as compared to females (18.6 ± 2.3 and 17.8 ± 2.2), respectively ($P < 0.001$).

The distances between VC and FR were slightly greater in males than females, though this difference was not statistically significant. A similar comparative study by Inal *et al.*^[8] also showed that the distance between FR and VC was greater in males in comparison to females.

Anatomy of the SS

As SS is a natural corridor of access during endonasal surgeries, many attempts have been made to delineate its anatomy with the help of CT scans.^[1,3,6,9,12,14,17,20] One of the most important features to be assessed in a preoperative CT scan is the pneumatization pattern of SS. In the sagittal plane, pneumatization of SS has been traditionally classified into conchal, presellar, sellar, and postsellar types.^[23] In the conchal type, the part below the sella is completely ossified with no air cavity. In the presellar type, pneumatization does not extend beyond the vertical line passing via the anterior clinoid. In the sellar type, pneumatization extends to a point between two lines described earlier, and it is called post-sellar when there is an extension beyond the posterior line.^[7,23] In our study, the post-sellar variant was predominant and was seen in 57.9% ($n = 274$), followed by the sellar variant in 24.3% ($n = 115$). The presellar and conchal were found in 17.6% ($n = 83$) and 0.2% ($n = 1$), respectively [Table 4].

Sareen *et al.*^[19] found a presellar variant in 75% and a sellar pattern in 25% of their cases. The pneumatization of the SS can extend to the greater wing, lesser wing, and basiocciput, and depending on the thickness of the lateral wall of the SS, the carotid artery can be found in close relation or within the SS.^[22] Cho *et al.*^[5] studied the degree of pneumatization of SS and bulging of vital adjacent neurovascular structures and found the following percentages of bulging, including the optic nerve, ICA, maxillary, and Vidian nerves 56%, 40%, 41%, and 52%, respectively. The bulging of neurovascular structures into SS directly correlated with the degree of pneumatization and increased risk of intraoperative injury.

The lateral sphenoid recess pneumatization is important in approaches to access the cavernous sinus, middle fossa, and petrous apex.^[12,14,16] SS pneumatization in the coronal plane has been classified by Mohebbi *et al.*^[14] as lateral recess, tangent, and less pneumatized based on a line connecting the FR to the VC. In our series, lateral recess pneumatization was defined as extending beyond the line connecting FR and VC and was seen in 14.6% ($n = 69$) of the patients on the right side and 15.4% ($n = 73$) on the left side. The pneumatization beyond the lateral recess into the greater wing of the sphenoid or clinoid process was

observed in 2.5% ($n = 12$) on the right and 4.5% ($n = 21$) on the left side [Table 5].

CONCLUSION

The results of our study can be utilized for a better understanding of the anatomy of the skull base. In skull base pathologies with distorted anatomical landmarks, a basic understanding of their interrelations can be used to have a better anatomical orientation. All these measures can help in avoiding complications and make EEAs safe.

Ethical approval

The research/study was approved by the Institutional Review Board at All India Institute of Medical Sciences, New Delhi, number IEC-415/06.05.22, dated 09-05-2022.

Declaration of patient consent

Patients' consent not required as patients' identities were not disclosed or compromised.

Financial support and sponsorship

Nil.

Conflicts of interest

There are no conflicts of interest.

Use of artificial intelligence (AI)-assisted technology for manuscript preparation

The authors confirm that there was no use of artificial intelligence (AI)-assisted technology for assisting in the writing or editing of the manuscript and no images were manipulated using AI.

REFERENCES

- Açar G, Çiçekcibaşı AE, Çukurova İ, Özen KE, Şeker M, Güler İ. The anatomic analysis of the vidian canal and the surrounding structures concerning vidian neurectomy using computed tomography scans. *Braz J Otorhinolaryngol* 2017;85:136-43.
- Adin ME, Ozmen CA, Aygun N. Utility of the vidian canal in endoscopic skull base surgery: Detailed anatomy and relationship to the internal carotid artery. *World Neurosurg* 2019;121:e140-6.
- Bansberg SF, Harner SG, Forbes G. Relationship of the optic nerve to the paranasal sinuses as shown by computed tomography. *Otolaryngol Head Neck Surg* 1987;96:331-5.
- Chin OY, Ghosh R, Fang CH, Baredes S, Liu JK, Eloy JA. Internal carotid artery injury in endoscopic endonasal surgery: A systematic review. *Laryngoscope* 2016;126:582-90.
- Cho JH, Kim JK, Lee JG, Yoon JH. Sphenoid sinus pneumatization and its relation to bulging of surrounding neurovascular structures. *Ann Otol Rhinol Laryngol* 2010;119:646-50.
- Citardi MJ, Gallivan RP, Batra PS, Maurer CR Jr., Rohlfing T, Roh HW, *et al.* Quantitative computer-aided computed tomography analysis of sphenoid sinus anatomical relationships. *Am J Rhinol* 2004;18:173-8.
- Famurewa OC, Ibitoye BO, Ameye SA, Asaleye CM, Ayoola OO, Onigbinde OS. Sphenoid sinus pneumatization, septation, and the internal carotid artery: A computed tomography study. *Niger Med J* 2018;59:7-13.
- Inal M, Muluk NB, Arıkan OK, Şahin S. Is there a relationship between optic canal, foramen rotundum, and vidian canal? *J Craniofac Surg* 2015;26:1382-8.
- Kasemsiri P, Solares CA, Carrau RL, Prosser JD, Prevedello DM, Otto BA, *et al.* Endoscopic endonasal transpterygoid approaches: Anatomical landmarks for planning the surgical corridor. *Laryngoscope* 2013;123:811-5.
- Kassam AB, Vescan AD, Carrau RL, Prevedello DM, Gardner P, Mintz AH, *et al.* Expanded endonasal approach: Vidian canal as a landmark to the petrous internal carotid artery. *J Neurosurg* 2008;108:177-83.
- Mason EC, Hudgins PA, Pradilla G, Oyesiku NM, Solares CA. Radiographic analysis of the vidian canal and its utility in petrous internal carotid artery localization. *Oper Neurosurg (Hagerstown)* 2018;15:577-83.
- Mato D, Majime Y, Seiichiro H, Juan M, Naokatsu S. The vidian canal: Radiological features in Japanese population and clinical implications. *Neurol Med Chir (Tokyo)* 2015;55:71-6.
- Meng QG, Lu YT, Wang CX, Tan SP, Wei MH. Visualization of the vomerovaginal canal during endonasal transpterygoid approaches and CT imaging diagnosis. *J Anat* 2019;235:246-55.
- Mohebbi A, Rajaeih S, Safdarian M, Omidian P. The sphenoid sinus, foramen rotundum and vidian canal: A radiological study of anatomical relationships. *Braz J Otorhinolaryngol* 2017;83:381-7.
- Osawa S, Rhoton AL, Seker A, Shimizu S, Fujii K, Kassam AB. Microsurgical and endoscopic anatomy of the vidian canal. *Neurosurgery* 2009;64(5 Suppl 2):385-411; discussion 411-2.
- Oyama K, Tahara S, Hirohata T, Ishii Y, Prevedello DM, Carrau RL, *et al.* Surgical anatomy for the endoscopic endonasal approach to the ventrolateral skull base. *Neurol Med Chir (Tokyo)* 2017;57:534-41.
- Papavasileiou G, Hajjiannou J, Kapsalaki E, Bizakis I, Fezoulidis I, Vassiou K. Vidian canal and sphenoid sinus: An MDCT and cadaveric study of useful landmarks in skull base surgery. *Surg Radiol Anat* 2020;42:589-601.
- Pinheiro-Neto CD, Fernandez-Miranda JC, Rivera-Serrano CM, Paluzzi A, Snyderman CH, Gardner PA, *et al.* Endoscopic anatomy of the palatovaginal canal (palatosphenoidal canal): A landmark for dissection of the vidian nerve during endonasal transpterygoid approaches. *Laryngoscope* 2012;122:6-12.
- Sareen D, Agarwal AK, Kaul JM, Sethi A. Study of sphenoid sinus anatomy in relation to endoscopic surgery. *Int J Morphol* 2005;23:261-6.

20. Vaezi A, Cardenas E, Pinheiro-Neto C, Paluzzi A, Branstetter BF, Gardner PA, *et al.* Classification of sphenoid sinus pneumatization: Relevance for endoscopic skull base surgery. *Laryngoscope* 2015;125:577-81.
21. Vescan AD, Snyderman CH, Carrau RL, Mintz A, Gardner P, Branstetter B 4th, *et al.* Vidian canal: Analysis and relationship to the internal carotid artery. *Laryngoscope* 2007;117:1338-42.
22. Wang J, Bidari S, Inoue K, Yang H, Rhoton A. Extensions of the sphenoid sinus: A new classification. *Neurosurgery* 2010;66:797-816.
23. Yamashita S, Resende LA, Trindade AP, Zanini MA. A radiologic morphometric study of sellar, infrassellar and parasellar regions by magnetic resonance in adults. *Springerplus* 2014;3:291.

How to cite this article: Ganesh VL, Dharanipathy S, Pavana V, Kumar A, Sebastian L, Garg A. A computed tomography (CT)-based morphometric study of various skull base parameters and their anatomical relationships relevant to endoscopic endonasal skull base surgery. *Surg Neurol Int.* 2024;15:68. doi: 10.25259/SNI_1010_2023

Disclaimer

The views and opinions expressed in this article are those of the authors and do not necessarily reflect the official policy or position of the Journal or its management. The information contained in this article should not be considered to be medical advice; patients should consult their own physicians for advice as to their specific medical needs.